Chapter 1

Introduction

1.1 Background

The traditional viewpoint of animal-fluid interactions research is to arrive at a mechanistic understanding of factors that affect the distribution, ecology and energetics of swimming organisms. Generally in these studies, animal-fluid interactions are investigated to characterize propulsive strategies [78, 18, 82, 27], estimate cost of transport [106, 32, 76] and determine feeding processes such as ingestion rates and prey selection [121, 123, 129, 58]. These interactions are commonly investigated by using quantitative flow measurement techniques, which include digital particle image velocimetry, or DPIV [140, 133]. Due to limitations in quantitative flow measurements in the natural environment, animal measurements are conducted in laboratories. To increase measurement efficiency, quantitative lab techniques incorporate methods that limit or make animal motion more predictable [137, 4, 131]. These methods have been shown to have an altering impact on animal behavior and resulting flow fields [10, 14]. Hence, it is reasonable to question conclusions made about the impact of background flows in the field from measurements conducted in a laboratory environment. Therefore, an apparatus that will enable the quantitative measurement of flows surrounding a swimming animal in the field is needed to accurately address the effect of background flows on animal swimming and fluid transport.

Quantitative field measurements using DPIV techniques have been achieved in the past. Submersible PIV systems have been designed to measure turbulence levels in the bottom ocean boundary

layer, mean vertical velocity profiles, microscale turbulence structures and time evolution of the mean velocity in coastal and river environments [7, 90, 118, 17]. However, existing field DPIV devices lack the functionality required to collect quantitative measurements of animal-fluid interactions. Additionally, these devices are unable to actively track the movement of animals in real-time due to their large size, lack of agility and controllability and physical connections to a ship or shore. Moreover, most of these systems are unavailable to most researchers in the field due to their deployment mechanisms (i.e., requiring a research vessel) and cost to build. We describe the development of a self-contained underwater velocimetry apparatus, or SCUVA, that achieves the goal of real-time, quantitative field measurements of aquatic animal-fluid interactions [66]. Using SCUVA, we obtain measurements of flow fields surrounding animals in the field and analyze the effect of background flows on swimming animals. Using a dynamical systems technique called Lagrangian coherent structures (LCS; [54, 115, 114]) to quantitatively compare laboratory and field-generated flows, we find that background flow structures alter fluid transport by swimming jellyfish, which has particular relevance to feeding currents and prey selection by these animals. The ability to quantify background flows and their influence on animal-fluid interactions will allow us to broaden our concept of animal-fluid interactions to include the effects swimming animals have on their surrounding environment. Recent work reveals that such interactions may be more relevant than previously thought [67].

Recently, biogenic mixing has received attention in studies of diurnally migrating animals [59, 35]. Measurements of the turbulent kinetic energy dissipation show an increase in background turbulence levels during a migration of krill [74]. However, recent literature has found that if biogenic mixing relies on the interaction of wake structures and corresponding length scales, their actions are ineffective in a viscous, stratified environment [135]. We discovered a more effective mechanism for biogenic mixing called drift [67], which is active during animal swimming. As a sphere moves in potential flow, a volume of fluid (or drift volume) is displaced permanently in the direction of body motion and is equal to the product of the body volume and the body's associated coefficient of added mass [34]. In studies of a sphere moving in Stokes flow, the drift volume becomes infinite [39]. However, since animals operate in intermediary Reynolds number regimes, the behavior of drift

as viscosity is altered is unknown. We show that unlike mechanisms that rely on turbulent mixing generated by wake structures, drift is enhanced as viscous effects are increased. In addition, animal morphology and body shape cannot always be described as spherical or cylindrical, and consequently the effect of varying body shape needs to be addressed. While drift has been observed in jellyfish and copepods [67, 64], to understand its relevance in the global ocean the effects of stratification needs to be considered. Finally, we show that at buoyancy frequencies on the order of the mean ocean, fluid transport due to drift remains a powerful mechanism through which biogenic mixing may provide a significant contribution to mixing in the oceans.

1.2 Research Objectives

There are three main goals for this thesis. The first goal is to design and build an apparatus that can be used in the field to quantify animal-fluid interactions. At the time of this work, quantitative methods to measure the flow fields generated by swimming animals in their natural environment were not available. Using data collected from the field apparatus, we can accomplish the second goal, which is to apply robust dynamical systems techniques to understand the effect background flows have on swimming animals. The potential effects of background flows on swimming animals include variations in fluid transport with application to feeding and propulsive swimming modes. The third and final goal is to determine the dominant mechanisms of fluid transport utilized by swimming animals in the natural field setting. Depending on the mechanism, migrating animals may have potential to impact their surrounding aqueous environment.

1.3 Organization of Thesis

Chapter 2 describes the development and design of SCUVA and experimental methods that can be applied in conjunction with its use. Chapters 3 and 4 contain applications of quantitative measurements to animal-generated flows in the field. Chapter 5 investigates the effect of stratification on the fluid transport mechanism employed by small swimming animals. Chapter 6 presents a few

potential directions for this work that should be investigated in the future.

Most of the chapters in this thesis were formed from a series of published papers. However, an attempt has been made to integrate them so as to prevent redundancy. A list of papers used to develop chapters 2, 3, and 4 is shown below along with my contribution to each paper. Abstracts of these and other papers written during my doctoral tenure can be found in appendix C.

Chapter 2

K. Katija and J. O. Dabiri, (2008). In situ field measurements of aquatic animal-fluid interactions using a self-contained underwater velocimetry apparatus (SCUVA). *Limnol. Oceanogr. Meth.*, 6: 162–171.

My main contributions to this paper were preparing the draft, analyzing the PIV data and comparing the models for turbulent kinetic energy dissipation.

Chapter 3

K. Katija, S. P. Colin, J. H. Costello and J. O. Dabiri, Comparison of flows generated by swimming animals in the laboratory and in situ: A coherent structure analysis. In review.

My main contributions to this paper were preparing the draft and conducting the analysis to produce the results of all DPIV and LCS computations.

Chapter 4

K. Katija and J. O. Dabiri, (2009). A viscosity-enhanced mechanism for biogenic ocean mixing. *Nature*, 460: 624–626.

My main contributions to this paper were collecting the field data, analyzing the field data, running viscous simulations and helping to write the paper. Dr. Dabiri and my contributions to this paper were comparable.

Chapter 2

Development of Field Measurement Technique

2.1 Introduction

The ability to directly measure physical interactions between aquatic animals and the surrounding fluid environment is necessary to provide empirical data for studies in fields as diverse as oceanography, ecology, biology, and fluid mechanics. However, field measurements introduce practical challenges such as environmental conditions, animal availability, and the need for field-compatible measurement techniques. To avoid these challenges, scientists typically use controlled laboratory environments to study animal-fluid interactions.

To increase measurement efficiency, researchers have devised methods to constrain animal movement in the laboratory. These techniques include placing animals in flumes [37, 4, 131], tethering [137, 70, 32, 143], and conducting free-swimming measurements with imposed flow conditions [10, 113]. Traditional qualitative and quantitative measurement techniques include dye visualizations [36, 28] and digital particle image velocimetry (DPIV; [140, 37, 29]). The computation of Lagrangian coherent structures (LCS) from the DPIV data has been recently shown to provide a robust method for quantifying the features of the flow field [113, 97].

Despite the prevalent use of laboratory measurements, it is reasonable to question whether one can extrapolate natural behavior (i.e., that which occurs in the field) from laboratory measurements. For example, it is known that the presence of tethers alters the flow fields of ciliated larvae [43] and

affects the structure of LCS in the wake of a jellyfish [65]. Especially in unsteady swimming, boundary layer development and forces associated with overcoming the inertia of animal motion are altered when an animal is tethered. Catton et al. [14] found differences in the strain rate fields between free-swimming and tethered copepods and noted the importance of studying free-swimming animals when making sensory ecology conclusions. Hence, at least in these cases and likely in others, a quantitative field measurement technique is needed to correctly characterize in situ behavior.

Quantitative field measurements using DPIV techniques have been achieved previously. A potential constraint in the field is the need for particles to track in the flow to implement DPIV. In coastal water, suspended particulate matter exhibits sizes on the order of 10 μm in diameter and concentrations between 0.002 and 10 per mm^3 [1]. Additional studies using a submersible holocamera for particle detection confirmed a sufficient presence of seeding particles to perform DPIV in ocean water [68]. Submersible PIV systems have previously been designed to measure turbulence levels in the bottom ocean boundary layer, and to provide data on mean vertical velocity profiles and the time evolution of the mean velocity [7, 90]. Free-falling platforms using a combination of measurements from planar laser-induced fluorescence and stereoscopic PIV have been used to observe and quantify microscale turbulence structures in the upper ocean [118]. In addition to these larger (apparatus weight on the order of 103 kg) and more expensive submersible DPIV devices, it has recently been proposed to use a small-scale submersible PIV system to characterize naturally occurring flows close to the shore [17].

Existing field DPIV devices lack the functionality required to collect quantitative measurements of animal-fluid interactions. For example, these devices typically have physical connections (e.g., cables) between the submerged device and the surface, which limits the area that can be measured to a fixed radius around a surface connection point. Additionally, these devices are usually unable to actively track the movement of animals in real-time due to their large size and lack of agility and controllability. Hence, existing systems are typically kept in a stationary position, towed behind a vessel, or programmed to execute predefined sweeps for data collection. A self-contained, portable device that can actively track animals independent of any connection to the surface and that is able

to provide quantitative measurements of the flow field surrounding an animal has not previously been developed to the best of the authors knowledge. Here, we describe the development of a self-contained underwater velocimetry apparatus, or SCUVA, that achieves the goal of real-time, quantitative field measurements of aquatic animal-fluid interactions.

To demonstrate the developed method, we conducted a preliminary investigation of the potential role of animal-fluid energy interactions in ocean mixing, a topic of increasing study that has been limited by the need for in situ field data at the scale of individual animals. Mixing against ocean stratification requires an input of mechanical energy whose sources are traditionally attributed primarily to winds and tides [89]. Biological sources of ocean mixing continued to be overlooked until rates of kinetic energy production were calculated for representative species of schooling animals [59]. The biological rate of kinetic energy production of a broad range of schooling animals was found to be on the order of 10^{-5} W kg^{-1}, which was later confirmed by microscale shear measurements of a large concentration of krill [74]. These findings suggest that biosphere input to the ocean mixing energy budget may impact mixing at the same level as winds and tides, whose respective rates of kinetic energy production are of the same order [35]. However, the issue of biogenic mixing remains largely unresolved. To assess the potential of SCUVA to inform the ongoing debate regarding biogenic turbulent mixing, we study the dynamics of *Aurelia labiata* swimming in coastal regions near Long Beach, California. SCUVA measurements of *Aurelia* are used to directly quantify the kinetic energy in the flow field induced by the swimming motions of individual medusae. The results are compared with the semi-empirical model predictions of Huntley and Zhou [59].

2.2 Experimental Methods

Specimens of juvenile *Aurelia labiata*, an oblate hydromedusa, were imaged using SCUVA off the coast of Long Beach, CA, USA (lat 33.76^o N, long 118.12^o W) during the month of March 2007. Dives were conducted at night to ensure that the DPIV laser sheet was minimally affected by other light sources. All data were collected in shallow water (depths less than 5 m). Relying on the presence of natural sedimentation to provide sufficient seeding density for DPIV, a single representative jellyfish

swimming cycle (duration of 1 s) was analyzed in detail. The images captured by SCUVA were processed with an in-house DPIV algorithm. The time between successive images (dt) was 0.033 s. The DPIV interrogation window size was 32×32 pixels with a 50% overlap (16×16 pixel step size). The velocity and vorticity calculations introduce measurement uncertainties of 5% and 7%, respectively (based on propagating error associated with the camera-laser system).

The body axis of a medusa swimming in the laser sheet is typically oriented at an angle θ with the horizontal. To simplify the subsequent data analyses, the instantaneous velocity fields were rotated by an angle $-\theta$ to align the animals body axis with the horizontal. Assuming radial flow symmetry (see appendix A for details), data within a cylinder of radius R surrounding the animal were then used to compute spatial integrals of the velocity field. Figure 2.1 illustrates this post-processing as applied to the velocity field at time $t = 0.633$ s after the start of a swimming cycle (i.e., the initiation of bell contraction). Figure 2.1(a) shows the raw image captured via SCUVA. The corresponding velocity field is shown in figure 2.1(b). The effect of camera motion can be seen in the relatively large velocity vectors that appear upstream from the animal where the real flow was relatively quiescent. These vectors are absent at the top and bottom of the field of view due to the lack of laser illumination in those regions; the width of the laser sheet is indicated by the abrupt transition from large to small velocity vectors at the upper and lower margins of the measurement window. Figure 2.1(c) shows the velocity field after the camera motion correction (i.e., equation (2.4)) is implemented and the data are rotated to orient the animal body axis horizontally. Finally, the integration area is identified in figure 2.1(d).

The velocity field in the selected cylindrical region of fluid around the animal was integrated to determine the instantaneous kinetic energy (E_{ke}) in the flow:

$$E_{ke}\,(t) = \frac{1}{2}\rho \int_V u_{real}^2\,(t)\; dV. \tag{2.1}$$

Since the animal is the only object in the region V and net advection through the region is observed to be small, it can be inferred that increases in the local kinetic energy are due to the swimming motions of the animal. Therefore, we can deduce the transient energetic effects of the animal-fluid

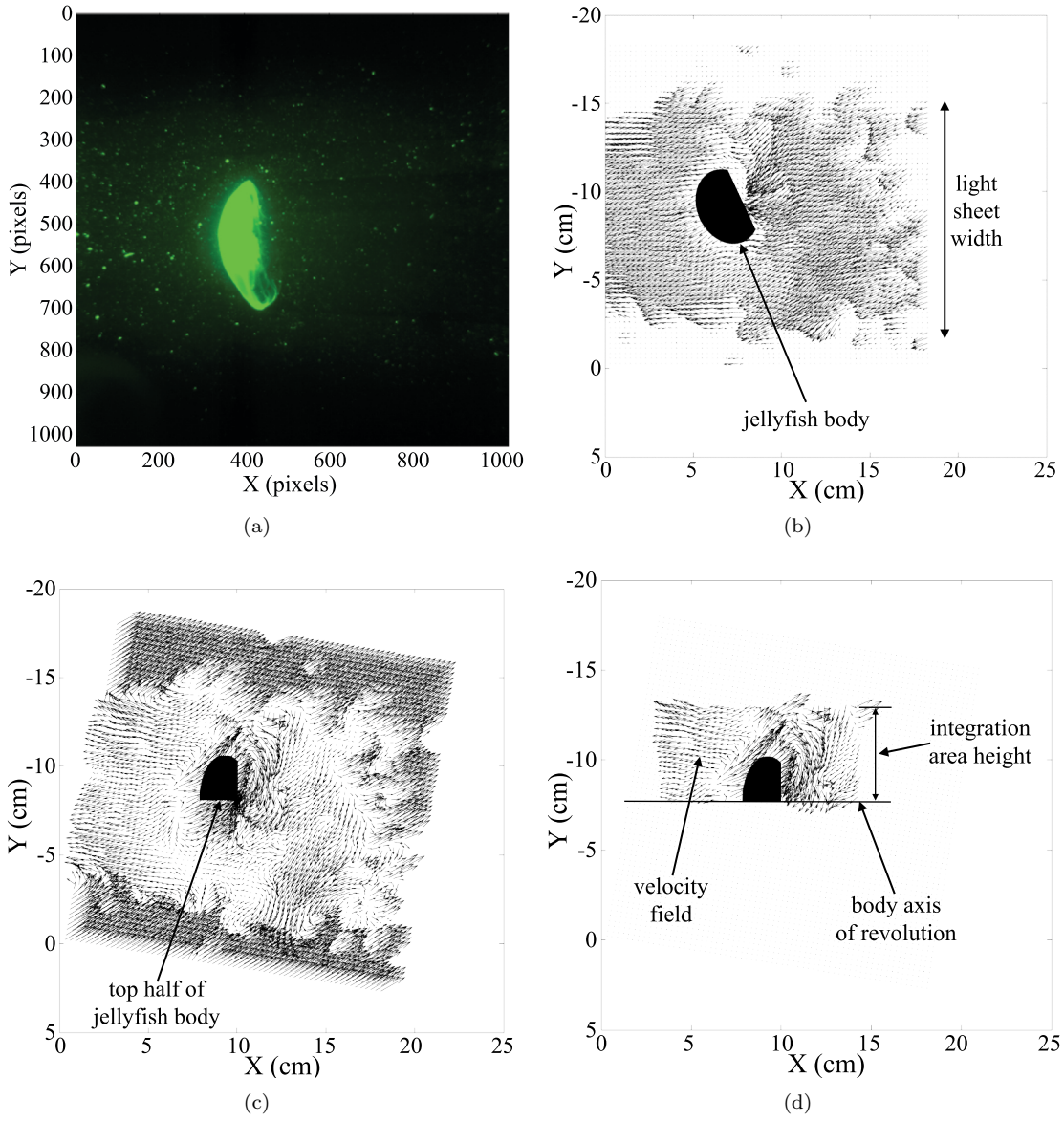

Figure 2.1. Velocity field corrections/adjustments to aid in the fluid energy computation:(a) Raw image captured by SCUVA at time $t = 0.633$ s; (b) Unrotated velocity field at time $t = 0.633$ s. (c) Rotated and corrected (using equation (2.2)) velocity field at time $t = 0.633$ s; (d) Rotated and corrected velocity field isolated to the energy integration area at time $t = 0.633$ s.

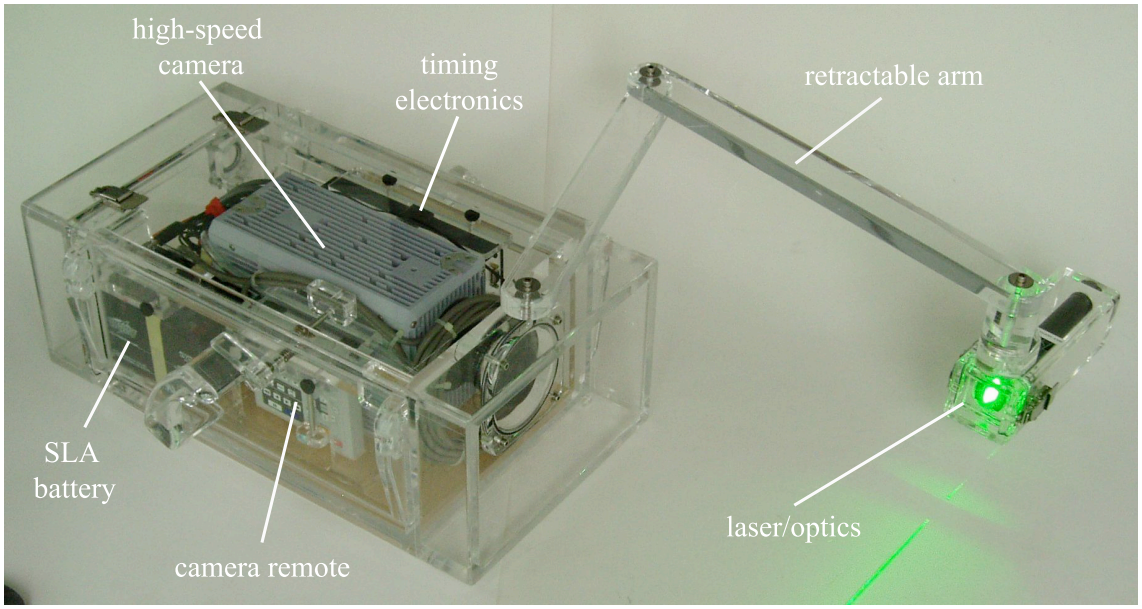

Figure 2.2. SCUVA shown with laser arm extended and laser sheet activated.

interaction by using the SCUVA measurements.

2.2.1 Components of the Field Apparatus

Particle illumination by SCUVA is provided by a continuous 300 mW, 532 nm solid-state laser. The output laser beam is collimated into a planar sheet by a planoconcave cylindrical lens (effective focal length = −6 mm). Using the current optical configuration, the size of the illuminated region can be adjusted from 15 cm W × 15 cm H to as large as 60 cm W × 60 cm H. Still smaller or large viewing windows can be achieved by modifying the camera lens and laser position. The laser and optics are mounted in a waterproof housing at the end of a retractable arm that locks to ensure that the camera is focused on the plane of the laser sheet at all times (figure 2.2; diagrams can be found in appendix B). The arm is collapsed while the SCUBA diver swims to the measurement site and subsequently extended to initiate measurements.

The flow field illuminated by the laser sheet is imaged by a high-speed camera (Photron APX-RS). The camera records images at a maximum resolution of 1024 × 1024 pixels at speeds up to 3000 frames s^{-1}. Higher speed recordings can be made at reduced spatial resolution. An electronic

shutter enables exposure times as short as 10^{-6} s, ensuring that particles can be imaged without any blurring. Recorded images are stored internally on an 8 GB hard drive. This capacity enables collection of 6144 full-resolution frames before the device must be surfaced to upload the stored measurement data. Control of the camera is achieved by a single START-STOP push-button control integrated into the right handle of the main housing containing the camera. The camera is moisture resistant and shock rated up to 100 g (980 m s^{-2}).

In order to measure a broad range of flow speeds in situ, timing electronics (Signal Forge 1000) have been integrated to ensure that particle displacements between adjacent frames can be optimally captured regardless of flow conditions. These electronics send a TTL trigger signal to the camera to initiate each image capture event. The duration between input trigger signals is made shorter for faster flow (i.e., so that particles do not travel too far in between frames) and longer for slower flow (i.e., so that a measurable change in particle position is achieved). The timing electronics are programmed on the boat/shore prior to initiating a dive.

The laser is powered by a rechargeable lithium-ion battery with a lifetime of 60 min starting from a full charge. This is sufficient for individual dive expeditions. In practice, several batteries are brought to the field so that recharging need not commence until after several dives. The camera and timing electronics are powered by a single 12 V, 10 A sealed lead acid rechargeable battery. This battery lasts marginally longer than the laser battery, and hence dive duration is limited by the laser power. The housings (Sexton Photographics) for the camera and laser are both constructed from impact-resistant acrylic to ensure durability while maintaining relatively light weight and visual access to the SCUVA components. The retractable arm connecting the two housings is also constructed from acrylic (dimensions can be found in appendix B). The rear of the camera housing contains several interfaces that enable interaction with the camera and battery without removing them from the housing. These include a gigabit ethernet link for data transfer to/from the camera, outlet for battery recharging, and on-off switches for the camera and timing electronics. In addition, a pair of one-way gas valves enable the air within the camera housing to be purged. This is useful for replacing ambient humid air with dry air, thereby reducing the effects of moisture condensation

within the housing when it is submerged in cold water. Both the laser and camera housing can withstand water pressures at depths up to 40 m (4 atm gage pressure). Figure 2.3 shows images from a demonstration of SCUVA in a swimming pool. For scale reference, the diver in this demonstration is 1.63 m tall.

2.2.2 Additional Considerations for Field Data

The velocity field captured by SCUVA (u_{scuva}) includes the actual motion of the fluid (u_{real}) as well as undesired motion of the camera (u_{camera}) that occurs due to movement of the diver during the measurements,

$$u_{scuva} = u_{real} + u_{camera}. \tag{2.2}$$

Since the camera is rigid, it possesses six degrees of freedom in its motion: translation along three orthogonal axes in space, and rotation about those three axes. Therefore, its velocity field u_{camera} is either spatially uniform (i.e., a constant) throughout the camera field of view, in the case of linear camera motion; or, a linear function of position within the camera field of view, in the case of rotational camera motion; or, a superposition of these two. This component u_{camera} of the measured velocity field must be subtracted from the SCUVA measurements to obtain the true fluid motion.

Before describing the motion correction that was implemented, it is worth noting that physically relevant derivatives of the measured velocity field (u_{scuva}) are either insensitive to the camera motion or else they explicitly indicate the effect of the camera motion. For example, in the case of linear camera motion, the measured vorticity field ω_{scuva} is equal to the real vorticity field ω_{real}, irrespective of the linear camera motion. This is because the vorticity field is determined by taking the mathematical curl of the velocity field, and the curl of the spatially uniform vector u_{camera} is identically zero. Hence, ω_{camera} is always equal to zero for linear camera motion. In the case of rotational camera motion, u_{camera} adds a rigid-body rotation to the real fluid motion. Hence, the vorticity ω_{camera} associated with rotational camera motion appears as a spatially uniform background vorticity (i.e., a constant vector) on top of which the real fluid vorticity is superimposed. By determining the level of background vorticity in regions away from the animal, this effect can be

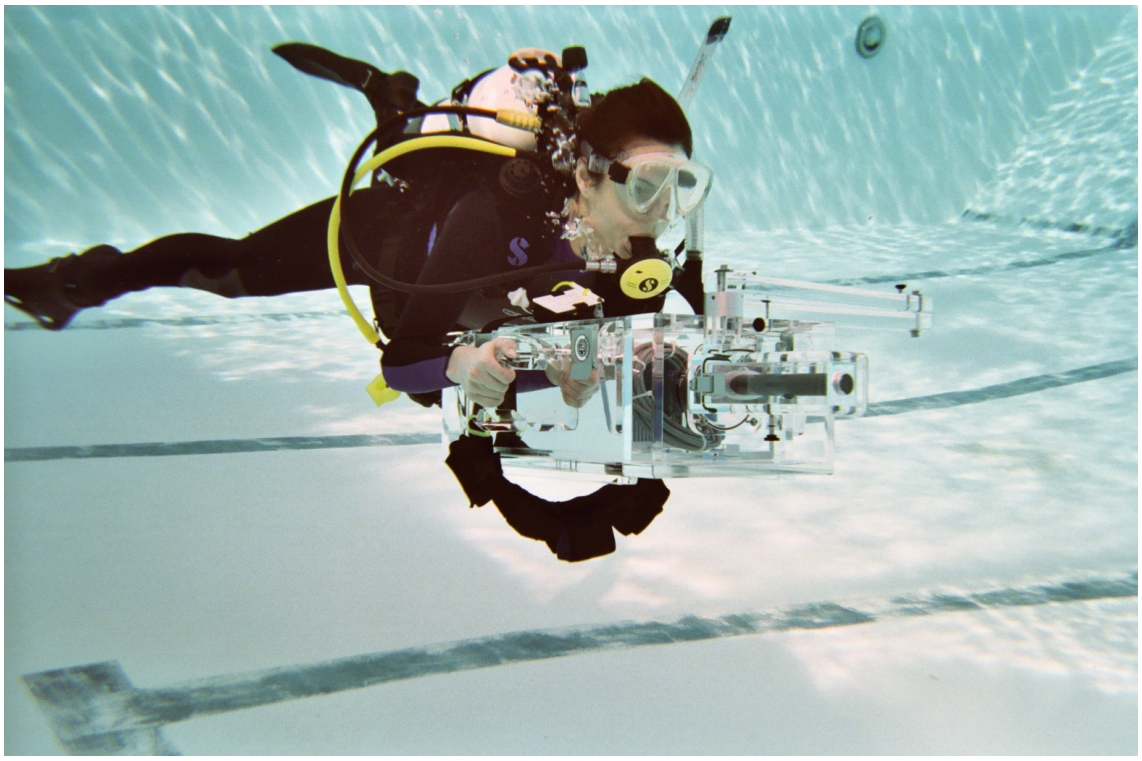

(a) SCUVA with the laser arm in the stowed position

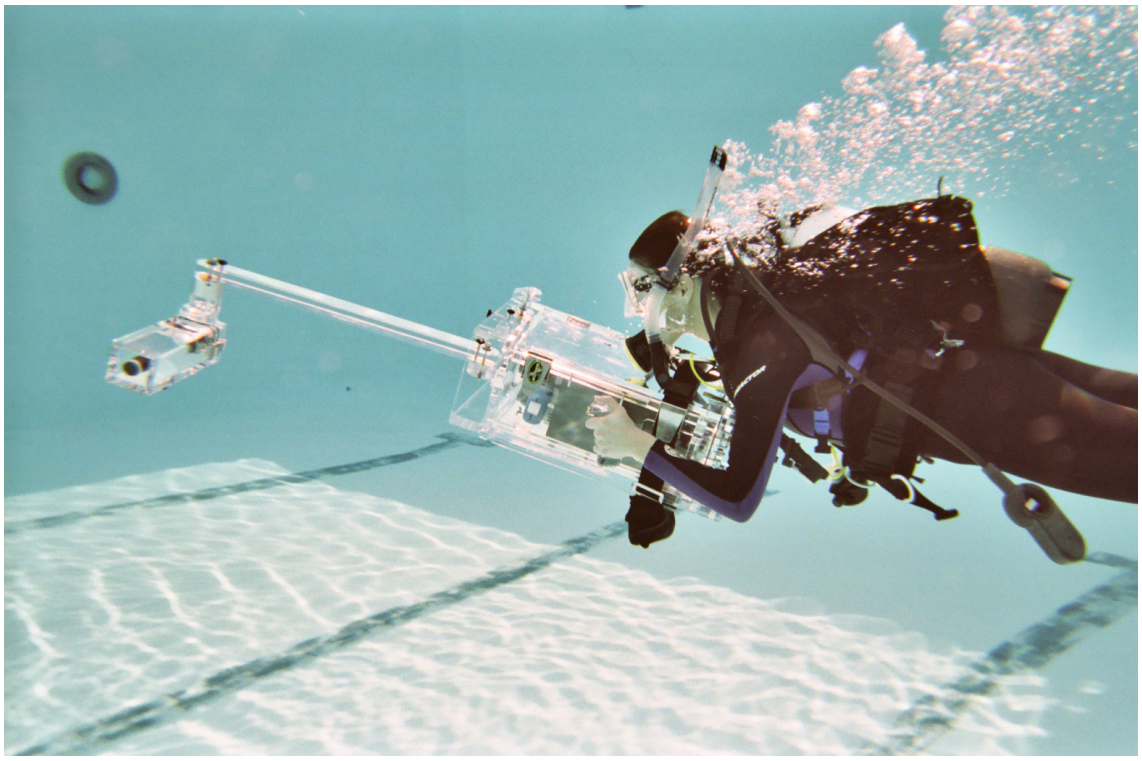

(b) SCUVA with the laser arm in the deployed position

Figure 2.3. Selected images from a swimming pool demonstration of SCUVA.

subtracted from the measurements. Notably, flow analyses based on Lagrangian coherent structures (LCS; [113, 97]) are inherently insensitive to both linear and angular camera motion because these constitute transformations of reference frame to which LCS are invariant by definition [54]. To be sure, the effect of linear camera motion on the velocity field measurements can be corrected in an approximate fashion by first noting that in a volume V of fluid with rigid walls or in an unbounded flow ($V \to \infty$) that is at rest at infinity,

$$\overline{u_{real}} = 0, \tag{2.3}$$

where the overbar denotes a spatial average over the volume [116]. Taking the spatial average of equation (2.2) over the volume and applying equation (2.3),

$$\overline{u_{scuva}} = \overline{u_{camera}} = u_{camera},$$

since u_{camera} is spatially uniform for linear motions of the camera. Hence,

$$u_{real} \approx u_{scuva} - \overline{u_{scuva}}. \tag{2.4}$$

Equation (2.4) is presented as an approximation because strict equality only holds in the aforementioned cases of a bounded flow with rigid walls or in a flow at rest at infinity. By contrast, the SCUVA measurements capture only a small subset of the bounded flow (i.e., the landlocked marine environment), and although the flow may be at rest far from the animal, the total volume of fluid measured in the field of view is finite. The error associated with the correction is dependent on the animal size relative to the viewing window and on the spatial average of the velocity field that the animal creates. To see this, first note that the contributions from the velocity field of the animal (u_{real}) and the camera motion (u_{camera}) to the spatially averaged velocity field measured by SCUVA (u_{scuva}) are given by

$$\overline{u_{scuva}} = \frac{1}{A_{window}} \int_{window} (u_{real} + u_{camera})\, dA,$$

where A_{window} is the area of the measurement window and the effect of spatially uniform currents

through the measurement window is included in u_{camera}. If we assume that the velocity field of the animal dominates a region of characteristic area A_{animal} in the measurement window, then equation (2.5) can be rewritten as

$$\overline{u_{scuva}} = \left(\frac{A_{window} - A_{animal}}{A_{window}}\right)\overline{u_{camera}} + \left(\frac{A_{animal}}{A_{window}}\right)\overline{u_{real}},$$

where the overbars indicate spatial averages of the velocity fields. From this relationship, we see that the camera motion correction given by equation (2.4) subtracts both the camera motion and a portion of the real velocity field created by the animal. This latter subtraction may be considered the error ϵ of the motion correction and can be expressed relative to the total error correction u_{scuva} as

$$\epsilon = \left(\frac{A_{animal}}{A_{window}}\right)\left(\frac{\overline{u_{real}}}{\overline{u_{scuva}}}\right).$$

This error becomes small if $A_{animal} \ll A_{window}$ (i.e., the region of flow created by the animal is small relative to the measurement window size) and/or if the average velocity of the flow created by the animal is small (i.e., $\overline{u_{real}} \ll \overline{u_{scuva}}$). The latter condition may be difficult to evaluate a priori, but could be estimated based on existing models for the swimming of the target species. For example, since the momentum of the fluid set into motion by an animal starting from rest will be approximately equal and opposite to the momentum of the swimming animal itself, the magnitude of $\overline{u_{real}}$ can be estimated in this case as

$$\overline{u_{real}} \sim \frac{A_{body}}{A_{animal}} U_{body},$$

where A_{body} is the area of the animal body in the field of view and U_{body} is the velocity that the animal achieves starting from rest.

Since the SCUVA measurements are based on two-dimensional DPIV, certain camera motions cannot be corrected by using equation (2.4) or any other method. Specifically, linear and/or angular motions of the camera that cause the flow to pass out of the plane of the laser sheet during a

measurement cannot be compensated because the out-of-plane flow results in particle loss in the DPIV image cross-correlation. Due to this limitation of two-dimensional DPIV, measurements must be conducted in a manner that minimizes out-of-plane motions of particles in the camera field of view. In practice, the light sheet must be oriented such that the target animal swims parallel to it. The scuba diver must be especially careful not to move the device forward or backward during the measurement; panning of the camera while maintaining the laser sheet in the same plane is allowable if necessary. The laser sheet is a useful indicator of out-of-plane motions since the location at which the laser sheet intersects the animal is clearly visible and will change in the event of out-of-plane motion. As with any measurement technique, the skill of the operator is refined with practice.

2.3 Computational Methods

Huntley and Zhou [59] proposed a model to estimate the kinetic energy transferred to the fluid surrounding an aquatic animal during locomotion. In this model, the rate of kinetic energy transfer e_d is defined as

$$e_d = D\, u_c,$$

where D is the hydrodynamic drag on the animal and u_c is the cruising speed of the swimming animal. The total drag D caused by flow separation, surface friction, and loss of energy in the wake of the animal is defined in their model as

$$D = \frac{1}{2}\rho\, u_c^2\, S_w\, C_D,$$

where ρ is the density of seawater ($\rho = 1025$ kg m^3), S_w is the average total wetted surface area, and C_D is the drag coefficient. We note that equation (2.5) neglects the unsteady effects of animal propulsion and utilizes average values only, which is a major limitation of the model [32]. The Huntley-Zhou model also utilizes the empirical result that, for turbulent flow, the drag coefficient of

a flat plate parallel to the flow is given by

$$C_D = 0.072\, Re^{-0.2},$$

where Re is the Reynolds number. Reynolds number is defined as $Re = \frac{u_c L}{\nu}$, where L is the characteristic length scale of the animal and ν is the kinematic viscosity of seawater ($\nu = 1.18 \times 10^{-6}$ m^2 s^{-1}).

Although the drag model of Huntley and Zhou [59] is simplified, it enables us to compare a broad range of aquatic species without concern for differences in morphology and kinematics. We use the same drag model here to provide a comparison with the SCUVA measurements. We assume that the medusa body can be modeled as an axisymmetric, truncated ellipsoid. Therefore, the parameter S_w corresponds to the average surface area of an equivalent truncated ellipsoid and the characteristic length L is the average exit diameter of the animal. Using these parameters and the measured swimming speed of the animal, the model predicts a kinetic energy transfer given by the integral of energy transfer rate e_d integrated with respect to time t:

$$E_d = \int e_d\, dt = 0.036\, \rho\, u_c^3\, S_w \left(\frac{u_c\, L}{\nu}\right)^{-0.2} t. \tag{2.5}$$

2.4 Results

Figure 2.4 shows a series of images taken by SCUVA during a single swimming cycle. A color map matching the 532 nm laser output has been added to the images to show what is seen by scuba divers operating SCUVA during a night dive. The jellyfish is swimming from right to left. The swimming cycle starts ($t = 0$ s) with the relaxation phase, where the bell exit begins to expand radially outward. At the end of the relaxation phase ($t = 0.6$ s), the animal's morphology reaches its most oblate form. At $t = 0.633$ s, the animal begins to contract its bell and continues to do so until the end of the swimming cycle. A series of images with the uncorrected and corrected velocity field can be found in figures 2.5 and 2.6, respectively. The measured velocity fields are qualitatively

consistent with laboratory measurements of *Aurelia aurita* [113, 48]; the significant background environmental flow features observed via SCUVA are necessarily absent from previous laboratory studies conducted in artificial flow environments.

The effect of the cylindrical integration region size on the fluid energy measurement can be seen in figure 2.7. The data points labeled top and bottom correspond to the selection of the integration area above and below the body axis, respectively. If the flow exhibits radial symmetry, integration of the top or bottom half of the flow field should yield the same result. For the integration height equal to the maximum bell radius over the swimming cycle R (top or bottom $1R$), there is asymmetry between the top and bottom flow fields that may reflect asymmetry in the animal swimming kinematics. As the integration height is increased to $3R$, we see that the flow becomes more symmetrical. This is expected since the contribution of the asymmetric animal motion to the total fluid energy decreases as the integration height increases. Increasing the integration height, however, includes kinetic energy from background flows that are independent of the animal's swimming motions. This results in an increase in the magnitude of kinetic energy as seen in figure 2.7.

In figure 2.8, we compare the SCUVA measurements (using an integration height of $2R$) with the Huntley-Zhou model (equation (2.5)). We find that direct SCUVA measurements of the energetics of animal-fluid interactions are consistent with the Huntley-Zhou model, and that the model may in fact underestimate the transient energetics. The model approximates the animal body shape as a flat plate, which yields a conservative estimate of C_D, especially in light of its neglect of unsteady fluid dynamics. The simplistic drag model is likely a main source of the underestimated kinetic energy input during swimming. Additionally, the model assumes that S_w and Re (L and u_c) are constant in time (using the averaged value over the duration of swimming), when in fact the quantities vary during the swimming cycle of a jellyfish due to morphology shape changes and the inherent unsteadiness in periodic motion. Neglecting these effects precludes the possibility of a time-dependent energy prediction by the Huntley-Zhou model.

Unlike the Huntley-Zhou model that predicts a steady, linear increase in kinetic energy over time, SCUVA measurements reveal nonlinear variations in kinetic energy of the fluid over a swimming

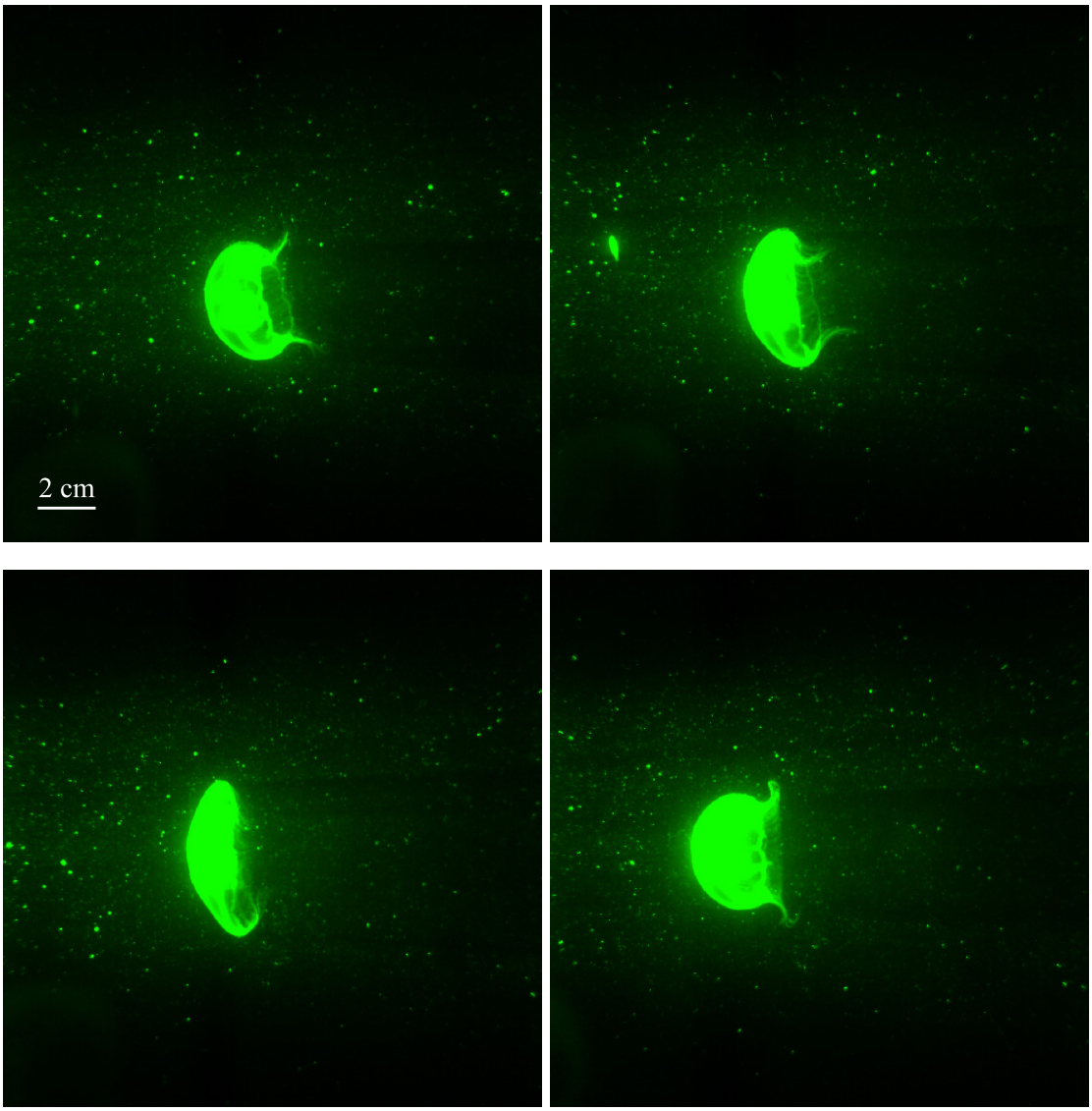

Figure 2.4. Selected images of a single swimming cycle captured by SCUVA at time (from left to right, top to bottom) $t = 0$ s, $t = 0.267$ s, $t = 0.533$ s and $t = 0.967$ s.

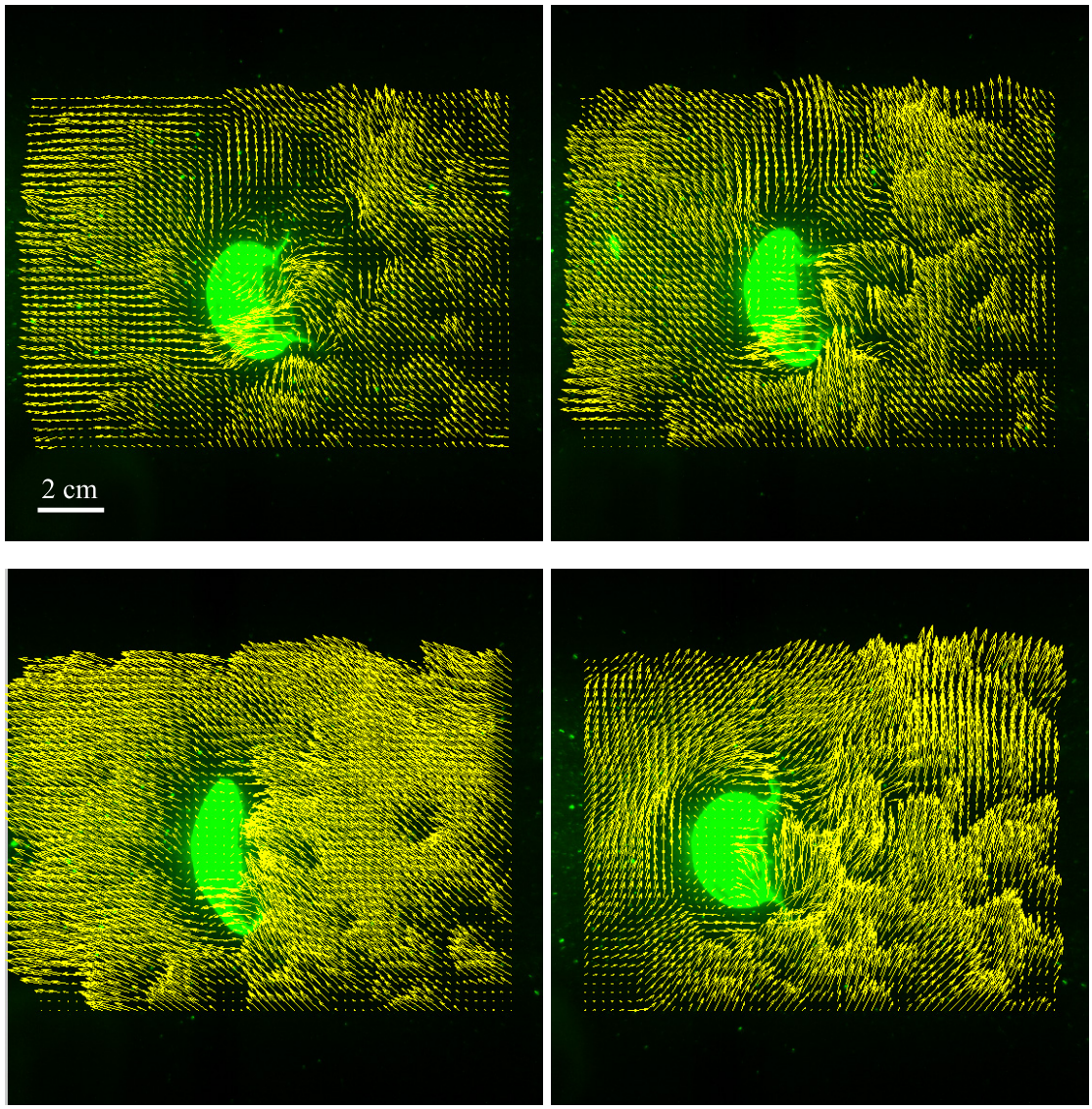

Figure 2.5. Uncorrected velocity fields at time (from left to right, top to bottom) $t = 0$ s, $t = 0.267$ s, $t = 0.533$ s and $t = 0.967$ s.

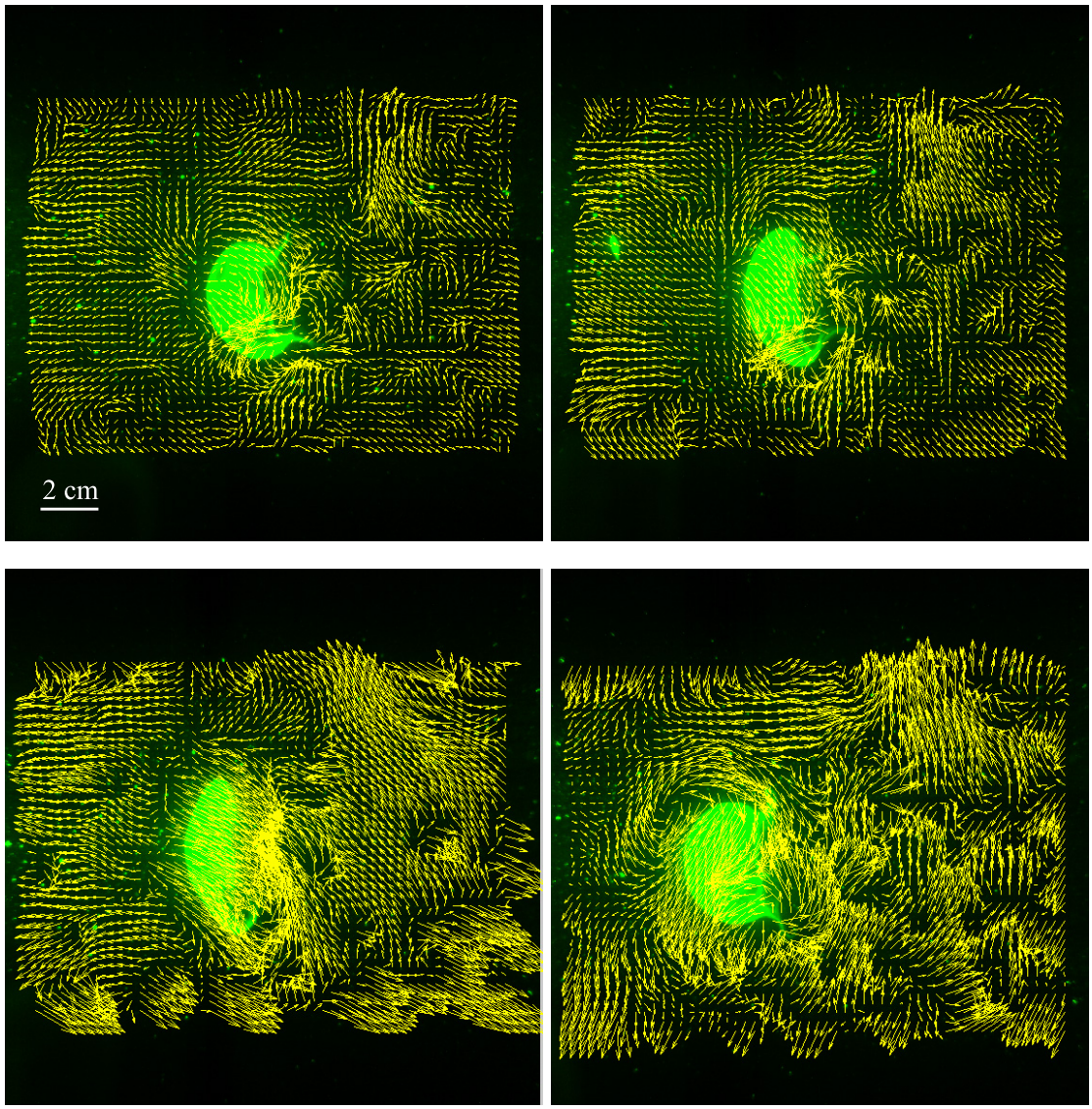

Figure 2.6. Corrected velocity fields at time (from left to right, top to bottom) $t = 0$ s, $t = 0.267$ s, $t = 0.533$ s and $t = 0.967$ s.

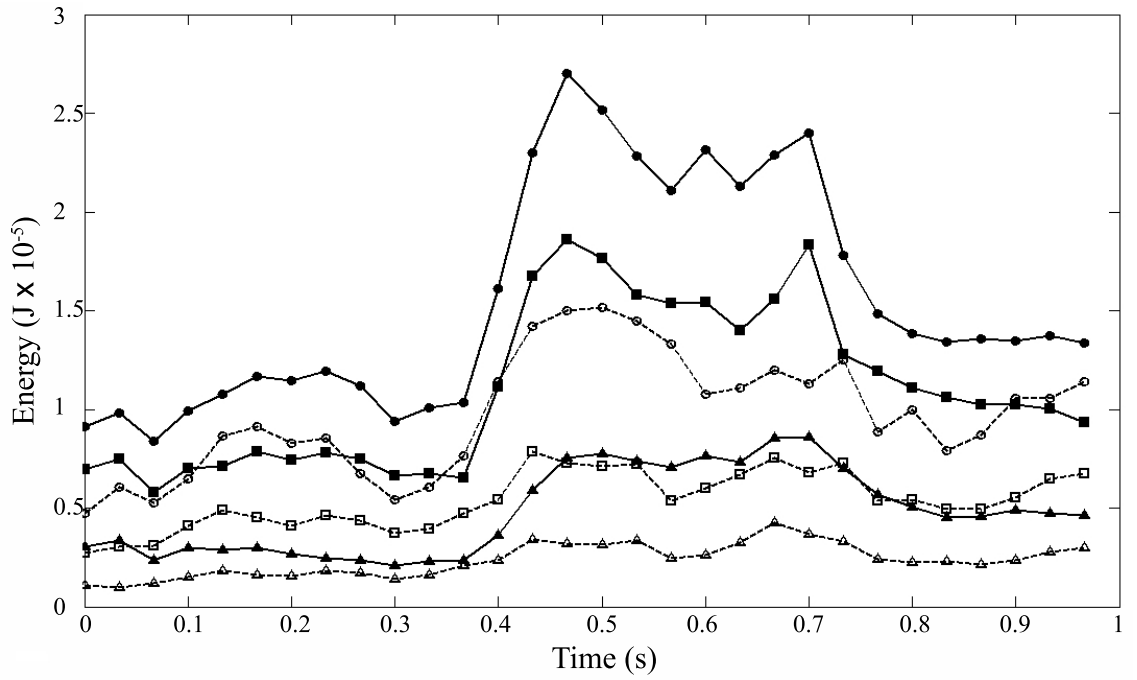

Figure 2.7. Comparison of the energy integration areas and their corresponding fluid energy values. Solid lines and filled symbols, top data; dashed lines and unfilled symbols, bottom data. Triangles, $1R$; squares, $2R$; circles, $3R$.

cycle. In the absence of energy dissipation, the kinetic energy measurements should be monotonically increasing with time, irrespective of linearity. However, we observe a drop in the kinetic energy toward the end of the measurements. We hypothesize that these dynamics are the result of kinetic energy dissipation in the flow that occurs between swimming cycles. The temporal trend of kinetic energy dissipation can be expected to follow an exponential decay in time [127], with characteristic time scale L/u_c

$$E_{ke}\,(t) = E_0\, exp\left[-B\,t\,\left(\frac{u_c}{L}\right)\right], \tag{2.6}$$

where E_0 is the initial kinetic energy and B is a constant of order one. Comparison of the SCUVA measurements with this predicted temporal behavior supports the conclusion that kinetic energy dissipation is prominent in this flow (figure 2.8). This result is relevant to the ocean-mixing problem because kinetic energy that is dissipated on fast time scales can only contribute to mixing in regions in very close proximity to the animal responsible for the energy input. In order to affect mixing in the entire ocean, kinetic energy generated in the wakes of swimming animals must persist for longer time

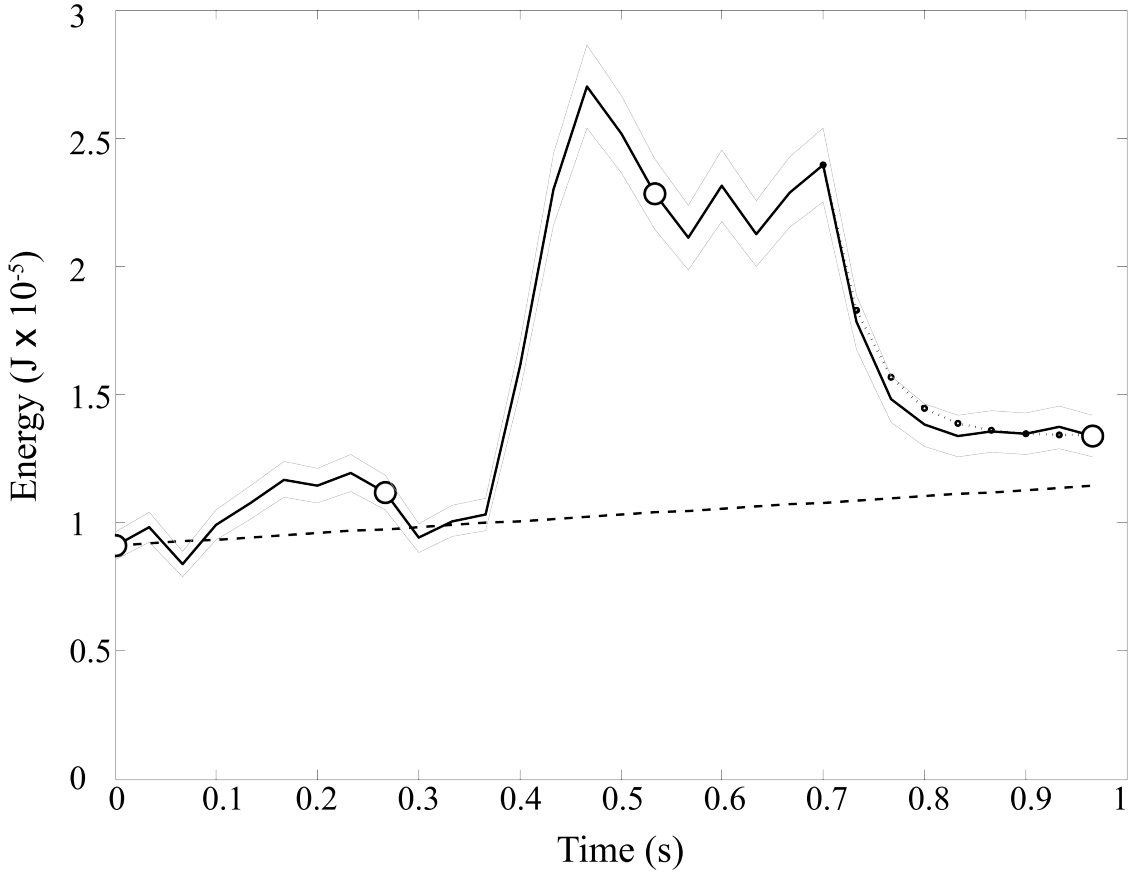

Figure 2.8. Comparison of Huntley and Zhou's predicted animal energy expenditure with SCUVA's computed fluid energy over a single swimming cycle. Dashed line, Huntley-Zhou model; solid black line, SCUVA energy computation; dotted line with empty circles, kinetic energy dissipation. Solid gray lines indicate upper and lower bounds of measurement uncertainty.

scales. As suggested by equation (2.6), this is only possible if the animal is large or swims at a slow velocity. This is a similar result as proposed by Visser [135] in that wake motions generated by small animals result in little mixing due to viscous scales in the flow, however wakes generated by larger animals will be able to mix a fluid more efficiently. Therefore, based on viscosity and dissipative arguments, wake structures generated by small animals cannot affect mixing in the global ocean due to the length and time scales at which they are active. Another transport mechanism aside from wake motions will need to be identified to support the case for biogenic mixing in the oceans. These hypotheses will require the support of additional empirical data before they can be accepted conclusively. SCUVA provides a means to achieve the necessary data.

2.5 Potential Applications for Field Apparatus

We have demonstrated the potential utility of SCUVA as a quantitative, laboratory-quality device to analyze animal-fluid interactions in the field. Although the present proof-of-concept focused specifically on energetic issues, the technique has the potential to provide much needed empirical data in cases where laboratory data cannot be obtained (e.g., due to animal fragility) and in cases where laboratory studies are insufficient to quantify animal-fluid interactions as they occur in situ. Examples of such studies include, but are not limited to, interspecific differences in foraging behavior, predator-prey encounters in a realistic turbulent media, energetics of locomotion, etc.

A unique challenge in the development of this technique is the lack of existing field data for many of the processes to be investigated using SCUVA. As such, validation of the SCUVA measurements necessarily relies on qualitative comparisons with laboratory measurements of similar processes. In the present case, we find that the velocity field immediately surrounding the swimming animal is similar to the velocity field measured in previous laboratory studies [113, 48]. However, the turbulent background flow is unique to field measurements since these environmental features are absent from controlled laboratory flows. This background flow is a significant feature of animal-fluid interactions in real marine environments, and SCUVA provides a means to quantify these local, transient features in real time. The effect of these background flows on animal-fluid interactions in

the field are discussed in chapter 3.

A potential obstacle to widespread use of this version of SCUVA is its cost. The apparatus described herein costs approximately 90K USD, primarily due to the specialized portable, high-speed camera that is used. However, in collaboration with Drs. J. H. Costello (Providence College) and S. P. Colin (Roger Williams University), we have since field-tested a smaller, second-generation version of SCUVA whose cost is reduced by more than an order of magnitude, to approximately 7K USD. This device uses an off-the-shelf camcorder (Sony HDR-HC7) within an underwater housing (Amphibico Dive Buddy EVO HD Elite) as the flow imager. This apparatus has a lower frame rate (60 fps standard, or 240 fps for up to 3 s), which may limit its ability to capture very fast fluid motions. Nonetheless, in our recent studies of fast-jetting medusan jellyfish that can swim up to 10 body lengths per second, we have not encountered cases in which camera speeds greater than 60 fps were necessary to resolve the flow. Additional benefits of the miniature SCUVA system are that it records to digital video (DV) tape, enabling continuous recording for up to 1 hr; it includes a built-in video display such that the operator can ensure the target organism is in the cameras field of view; and its size, weighing only 5 kg out of the water. A long-term study is underway using this second-generation device, the preliminary results of which are described in chapter 3 and 4. Images, diagrams and interface flow charts of all SCUVA design iterations are shown in appendix B.